

Wasserstein Adversarial Examples via Projected Sinkhorn Iterations

Eric Wong¹ Frank R. Schmidt² J. Zico Kolter^{3,4}

Abstract

A rapidly growing area of work has studied the existence of adversarial examples, datapoints which have been perturbed to fool a classifier, but the vast majority of these works have focused primarily on threat models defined by ℓ_p norm-bounded perturbations. In this paper, we propose a new threat model for adversarial attacks based on the Wasserstein distance. In the image classification setting, such distances measure the cost of moving pixel mass, which naturally cover “standard” image manipulations such as scaling, rotation, translation, and distortion (and can potentially be applied to other settings as well). To generate Wasserstein adversarial examples, we develop a procedure for projecting onto the Wasserstein ball, based upon a modified version of the Sinkhorn iteration. The resulting algorithm can successfully attack image classification models, bringing traditional CIFAR10 models down to 3% accuracy within a Wasserstein ball with radius 0.1 (i.e., moving 10% of the image mass 1 pixel), and we demonstrate that PGD-based adversarial training can improve this adversarial accuracy to 76%. In total, this work opens up a new direction of study in adversarial robustness, more formally considering convex metrics that accurately capture the invariances that we typically believe should exist in classifiers. Code for all experiments in the paper is available at https://github.com/locuslab/projected_sinkhorn.

1. Introduction

A substantial effort in machine learning research has gone towards studying *adversarial examples* (Szegedy et al., 2014), commonly described as datapoints that are indistinguishable

¹Machine Learning Department, Carnegie Mellon University, Pittsburgh, Pennsylvania, USA ²Bosch Center for Artificial Intelligence, Renningen, Germany ³Computer Science Department, Carnegie Mellon University, Pittsburgh, Pennsylvania, USA
⁴Bosch Center for Artificial Intelligence, Pittsburgh, Pennsylvania, USA. Correspondence to: Eric Wong <ericwong@cs.cmu.edu>.

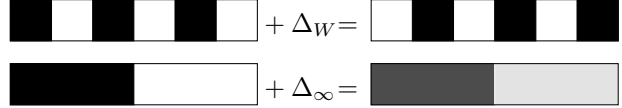


Figure 1. A minimal example exemplifying the difference between Wasserstein perturbations and ℓ_∞ perturbations on an image with six pixels. The top example utilizes a perturbation Δ_W to shift the image one pixel to the right, which is small with respect to Wasserstein distance since each pixel moved a minimal amount, but large with respect to ℓ_∞ distance since each pixel changed a maximal amount. In contrast, the bottom example utilizes a perturbation Δ_∞ which changes all pixels to be grayer. This is small with respect to ℓ_∞ distance, since each pixel changes by a small amount, but large with respect to Wasserstein distance, since the mass on each pixel on the left had to move halfway across the image to the right.

from “normal” examples, but are specifically perturbed to be misclassified by machine learning systems. This notion of indistinguishability, later described as the threat model for attackers, was originally taken to be ℓ_∞ bounded perturbations, which model a small amount of noise injected to each pixel (Goodfellow et al., 2015). Since then, subsequent work on understanding, attacking, and defending against adversarial examples has largely focused on this ℓ_∞ threat model and its corresponding ℓ_p generalization. While the ℓ_p ball is a convenient source of adversarial perturbations, it is by no means a comprehensive description of all possible adversarial perturbations. Other work (Engstrom et al., 2017) has looked at perturbations such as rotations and translations, but beyond these specific transforms, there has been little work considering broad classes of attacks beyond the ℓ_p ball.

In this paper, we propose a new type of adversarial perturbation that encodes a general class of attacks that is fundamentally different from the ℓ_p ball. Specifically, we propose an attack model where the perturbed examples are bounded in Wasserstein distance from the original example. This distance can be intuitively understood for images as the cost of moving around pixel mass to move from one image to another. Note that the Wasserstein ball and the ℓ_p ball can be quite different in their allowable perturbations: examples that are close in Wasserstein distance can be quite far in ℓ_p distance, and vice versa (a pedagogical example demonstrating this is in Figure 1).

We develop this idea of Wasserstein adversarial examples in two main ways. Since adversarial examples are typically best generated using variants of projected gradient descent, we first derive an algorithm that projects onto the Wasserstein ball. However, performing an exact projection is computationally expensive, so our main contribution here is to derive a fast method for *approximate* projection. The procedure can be viewed as a modified Sinkhorn iteration, but with a more complex set of update equations. Second, we develop efficient methods for adversarial training under this threat method. Because this involves repeatedly running this projection within an inner optimization loop, speedups that use a *local* transport plan are particularly crucial (i.e. only moving pixel mass to nearby pixels), making the projection complexity linear in the image size.

We evaluate the attack quality on standard models, showing for example that we can reduce the adversarial accuracy of a standard CIFAR10 classifier from 94.7% to 3% using a Wasserstein ball of radius 0.1 (equivalent to moving 10% of the mass of the image by one pixel), whereas the same attack reduces the adversarial accuracy of a model certifiably trained against ℓ_∞ perturbations from 66% to 61%. In contrast, we show that with adversarial training, we are able to improve the adversarial accuracy of this classifier to 76% while retaining a nominal accuracy of 80.7%. We additionally show, however, that existing *certified* defenses cannot be easily extended to this setting; building models provably robust to Wasserstein attacks will require fundamentally new techniques. In total, we believe this work highlights a new direction in adversarial examples: convex perturbation regions which capture a much more intuitive form of structure in their threat model, and which move towards a more “natural” notion of adversarial attacks.

2. Background and Related Work

Much of the work in adversarial examples has focused on the original ℓ_∞ threat model presented by Goodfellow et al. (2015), some of which also extends naturally to ℓ_p perturbations. Since then, there has been a plethora of papers studying this threat model, ranging from improved attacks, heuristic and certified defenses, and verifiers. As there are far too many to discuss here, we highlight a few which are the most relevant to this work.

The most commonly used method for generating adversarial examples is to use a form of projected gradient descent over the region of allowable perturbations, originally referred to as the Basic Iterative Method (Kurakin et al., 2017). Since then, there has been a back-and-forth of new heuristic defenses followed by more sophisticated attacks. To name a few, distillation was proposed as a defense but was defeated (Papernot et al., 2016; Carlini & Wagner, 2017), realistic transformations seen by vehicles were thought to be safe un-

til more robust adversarial examples were created (Lu et al., 2017; Athalye et al., 2018b), and many defenses submitted to ICLR 2018 were broken before the review period even finished (Athalye et al., 2018a). One undefeated heuristic defense is to use the adversarial examples in adversarial training, which has so far worked well in practice (Madry et al., 2018). While this method has traditionally been used for ℓ_∞ and ℓ_2 balls (and has a natural ℓ_p generalization), in principle, the method can be used to project onto any kind of perturbation region.

Another set of related papers are verifiers and provable defenses, which aim to produce (or train on) certificates that are provable guarantees of robustness against adversarial attacks. Verification methods are now applicable to multi-layer neural networks using techniques ranging from semi-definite programming relaxations (Raghunathan et al., 2018), mixed integer linear programming (Tjeng et al., 2019), and duality (Dvijotham et al., 2018). Provable defenses are able to tie verification into training non-trivial deep networks by backpropagating through certificates, which are generated with duality-based bounds (Wong & Kolter, 2018; Wong et al., 2018), abstract interpretations (Mirman et al., 2018), and interval bound propagation (Gowal et al., 2018). These methods have subsequently inspired new heuristic training defenses, where the resulting models can be independently verified as robust (Croce et al., 2018; Xiao et al., 2019). Notably, some of these approaches are *not* overly reliant on specific types of perturbations (e.g. duality-based bounds). Despite their generality, these certificates have only been trained and evaluated in the context of ℓ_∞ and ℓ_2 balls, and we believe this is due in large part to a lack of alternatives.

Highly relevant to this work are attacks that lie outside the traditional ℓ_p ball of imperceptible noise. For example, simple rotations and translations form a fairly limited set of perturbations that can be quite large in ℓ_p norm, but are sometimes sufficient in order to fool classifiers (Engstrom et al., 2017). On the other hand, adversarial examples that work in the real world do not necessarily conform to the notion of being “imperceptible”, and need to utilize a stronger adversary that is visible to real world systems. Some examples include wearing adversarial 3D printed glasses to fool facial recognition (Sharif et al., 2017), the use of adversarial graffiti to attack traffic sign classification (Eykholt et al., 2018), and printing adversarial textures on objects to attack image classifiers (Athalye et al., 2018b). While Sharif et al. (2017) allows perturbations that are physical glasses, the others use an ℓ_p threat model with a larger radius, when a different threat model could be a more natural description of adversarial examples that are perceptible on camera.

Last but not least, our paper relies heavily on the Wasserstein distance, which has seen applications throughout machine

learning. The traditional notion of Wasserstein distance has the drawback of being computationally expensive: computing a single distance involves solving an optimal transport problem (a linear program) with a number of variables quadratic in the dimension of the inputs. However, it was shown that by subtracting an entropy regularization term, one can compute approximate Wasserstein distances extremely quickly using the Sinkhorn iteration (Cuturi, 2013), which was later shown to run in near-linear time (Altschuler et al., 2017). Relevant but orthogonal to our work, is that of Sinha et al. (2018) on achieving distributional robustness using the Wasserstein distance. While we both use the Wasserstein distance in the context of adversarial training, the approach is quite different: Sinha et al. (2018) use the Wasserstein distance to perturb the underlying *data distribution*, whereas we use the Wasserstein distance as an attack model for perturbing each *example*.

Contributions This paper takes a step back from using ℓ_p as a perturbation metric, and proposes using the Wasserstein distance instead as an equivalently general but qualitatively different way of generating adversarial examples. To tackle the computational complexity of projecting onto a Wasserstein ball, we use ideas from the Sinkhorn iteration (Cuturi, 2013) to derive a fast method for an approximate projection. Specifically, we show that subtracting a similar entropy-regularization term to the projection problem results in a Sinkhorn-like algorithm, and using local transport plans makes the procedure tractable for generating adversarial images. In contrast to ℓ_∞ and ℓ_2 perturbations, we find that the Wasserstein metric generates adversarial examples whose perturbations have inherent structure reflecting the actual image itself (see Figure 2 for a comparison). We demonstrate the efficacy of this attack on standard models, models trained against this attack, and provably robust models (against ℓ_∞ attacks) on MNIST and CIFAR10 datasets. While the last of these models are not trained to be robust specifically against this attack, we observe that that some (but not all) robustness empirically transfers over to protection against the Wasserstein attack. More importantly, we show that while the Wasserstein ball does fit naturally into duality based frameworks for generating and training against certificates, there is a fundamental roadblock preventing these methods from generating non-vacuous bounds on Wasserstein balls.

3. Preliminaries

PGD-based adversarial attacks The most common method of creating adversarial examples is to use a variation of projected gradient descent. Specifically, let (x, y) be a datapoint and its label, and let $\mathcal{B}(x, \epsilon)$ be some ball around x with radius ϵ , which represents the threat model for the adversary. We first define the projection operator

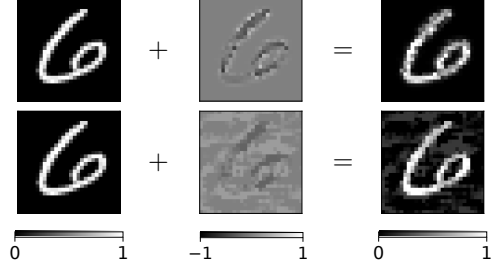


Figure 2. A comparison of a Wasserstein (top) vs an ℓ_∞ (bottom) adversarial example for an MNIST classifier (for $\epsilon = 0.4$ and 0.3 respectively), showing the original image (left), the added perturbation (middle), and the final perturbed image (right). We find that the Wasserstein perturbation has a structure reflecting the actual content of the image, whereas the ℓ_∞ perturbation also attacks the background pixels.

onto $\mathcal{B}(x, \epsilon)$ to be

$$\text{proj}_{\mathcal{B}(x, \epsilon)}(w) = \arg \min_{z \in \mathcal{B}(x, \epsilon)} \|w - z\|_2^2 \quad (1)$$

which finds the point closest (in Euclidean space) to the input w that lies within the ball $\mathcal{B}(x, \epsilon)$. Then, for some step size α and some loss ℓ (e.g. cross-entropy loss), the algorithm consists of the following iteration:

$$x^{(t+1)} = \text{proj}_{\mathcal{B}(x, \epsilon)} \left(x^{(t)} + \arg \max_{\|v\| \leq \alpha} v^T \nabla \ell(x^{(t)}, y) \right) \quad (2)$$

where $x^{(0)} = x$ or any randomly initialized point within $\mathcal{B}(x, \epsilon)$. This is sometimes referred to as projected *steepest descent*, which is used to generate adversarial examples since the standard gradient steps are typically too small. If we consider the ℓ_∞ ball $\mathcal{B}_\infty(x, \epsilon) = \{x + \Delta : \|\Delta\|_\infty \leq \epsilon\}$ and use steepest descent with respect to the ℓ_∞ norm, then we recover the Basic Iterative Method originally presented by Kurakin et al. (2017).

Adversarial training One of the heuristic defenses that works well in practice is to use adversarial training with a PGD adversary. Specifically, instead of minimizing the loss evaluated at a example x , we minimize the loss on an adversarially perturbed example x_{adv} , where x_{adv} is obtained by running the projected gradient descent attack for the ball $\mathcal{B}(x, \epsilon)$ for some number of iterations, as shown in Algorithm 1. Taking $\mathcal{B}(x, \epsilon)$ to be an ℓ_∞ ball recovers the procedure used by Madry et al. (2018).

Wasserstein distance Finally, we define the most crucial component of this work, an alternative metric from ℓ_p distances. The Wasserstein distance (also referred to as the Earth mover’s distance) is an optimal transport problem that can be intuitively understood in the context of distributions as the minimum cost of moving probability mass to change one distribution into another. When applied to images, this

Algorithm 1 An epoch of adversarial training for a loss function ℓ , classifier f_θ with parameters θ , and step size parameter α for some ball \mathcal{B} .

```

input: Training data  $(x_i, y_i), i = 1 \dots n$ 
for  $i = 1 \dots n$  do
    // Run PGD adversary
     $x_{adv} := x_i$ 
    for  $t = 1 \dots T$  do
         $\delta := \arg \max_{\|v\| \leq \alpha} v^T \nabla \ell(x_{adv}, y_i)$ 
         $x_{adv} := \text{proj}_{\mathcal{B}(x_i, \epsilon)}(x_{adv} + \delta)$ 
    end for
    // Backpropagate with  $x_{adv}$ , e.g. with SGD
    Update  $\theta$  with  $\nabla \ell(f_\theta(x_{adv}), y_i)$ 
end for

```

can be interpreted as the cost of moving pixel mass from one pixel to another another, where the cost increases with distance.

More specifically, let $x, y \in \mathbb{R}_+^n$ be two non-negative data points such that $\sum_i x_i = \sum_j y_j = 1$, so images and other inputs need to be normalized, and let $C \in \mathbb{R}_+^{n \times n}$ be some non-negative cost matrix where C_{ij} encodes the cost of moving mass from x_i to y_j . Then, the Wasserstein distance d_W between x and y is defined to be

$$d_W(x, y) = \min_{\Pi \in \mathbb{R}_+^{n \times n}} \langle \Pi, C \rangle \quad (3)$$

subject to $\Pi 1 = x, \Pi^T 1 = y$

where the minimization over transport plans Π , whose entries Π_{ij} encode how the mass moves from x_i to y_j . Then, we can define the Wasserstein ball with radius ϵ as

$$\mathcal{B}_W(x, \epsilon) = \{x + \Delta : d_W(x, x + \Delta) \leq \epsilon\} \quad (4)$$

4. Wasserstein Adversarial Examples

The crux of this work relies on offering a fundamentally different type of adversarial example from typical, ℓ_p perturbations: the Wasserstein adversarial example.

4.1. Projection onto the Wasserstein Ball

In order to generate Wasserstein adversarial examples, we can run the projected gradient descent attack from Equation (2), dropping in the Wasserstein ball \mathcal{B}_W from Equation (4) in place of \mathcal{B} . However, while projections onto regions such as ℓ_∞ and ℓ_2 balls are straightforward and have closed form computations, simply computing the Wasserstein distance itself requires solving an optimization problem. Thus, the first natural requirement to generating Wasserstein adversarial examples is to derive an *efficient* way to project examples onto a Wasserstein ball of radius ϵ . Specifically, projecting w onto the Wasserstein ball around x with radius

ϵ and transport cost matrix C can be written as solving the following optimization problem:

$$\begin{aligned} & \underset{z \in \mathbb{R}_+^n, \Pi \in \mathbb{R}_+^{n \times n}}{\text{minimize}} \quad \frac{1}{2} \|w - z\|_2^2 \\ & \text{subject to } \Pi 1 = x, \quad \Pi^T 1 = z \\ & \quad \langle \Pi, C \rangle \leq \epsilon \end{aligned} \quad (5)$$

While we could directly solve this optimization problem (using an off-the-shelf quadratic programming solver), this is prohibitively expensive to do for every iteration of projected gradient descent, especially since there is a quadratic number of variables. However, Cuturi (2013) showed that the standard Wasserstein distance problem from Equation (3) can be approximately solved efficiently by subtracting an entropy regularization term on the transport plan W , and using the Sinkhorn-Knopp matrix scaling algorithm. Motivated by these results, instead of solving the projection problem in Equation (5) exactly, the key contribution that allows us to do the projection efficiently is to instead solve the following entropy-regularized projection problem:

$$\begin{aligned} & \underset{z \in \mathbb{R}_+^n, \Pi \in \mathbb{R}_+^{n \times n}}{\text{minimize}} \quad \frac{1}{2} \|w - z\|_2^2 + \frac{1}{\lambda} \sum_{ij} \Pi_{ij} \log(\Pi_{ij}) \\ & \text{subject to } \Pi 1 = x, \quad \Pi^T 1 = z \\ & \quad \langle \Pi, C \rangle \leq \epsilon. \end{aligned} \quad (6)$$

Although this is an *approximate* projection onto the Wasserstein ball, importantly, the looseness in the approximation is only in finding the projection z which is closest (in ℓ_2 norm) to the original example x . All feasible points, including the optimal solution, are still within the actual ϵ -Wasserstein ball, so examples generated using the approximate projection are still within the Wasserstein threat model.

Using the method of Lagrange multipliers, we can introduce dual variables (α, β, ψ) and derive an equivalent dual problem in Lemma 3 (the proof is deferred to Appendix A.1).

Lemma 1. *The dual of the entropy-regularized Wasserstein projection problem in Equation (6) is*

$$\underset{\alpha, \beta \in \mathbb{R}^n, \psi \in \mathbb{R}_+}{\text{maximize}} \quad g(\alpha, \beta, \psi) \quad (7)$$

where

$$\begin{aligned} g(\alpha, \beta, \psi) = & -\frac{1}{2\lambda} \|\beta\|_2^2 - \psi\epsilon + \alpha^T x + \beta^T w \\ & - \sum_{ij} \exp(\alpha_i) \exp(-\psi C_{ij} - 1) \exp(\beta_j) \end{aligned} \quad (8)$$

Note that the dual problem here differs from the traditional dual problem for Sinkhorn iterates by having an additional

quadratic term on β and an additional dual variable ψ . Nonetheless, we can still derive a Sinkhorn-like algorithm by performing block coordinate ascent over the dual variables (the full derivation can be found in Appendix A.3). Specifically, maximizing g with respect to α results in

$$\arg \max_{\alpha_i} g(\alpha, \beta, \psi) = \log(x_i) - \log \left(\sum_j \exp(-\psi C_{ij} - 1) \exp(\beta_j) \right), \quad (9)$$

which is identical (up to a log transformation of variables) to the original Sinkhorn iterate proposed in Cuturi (2013). The maximization step for β can also be done analytically with

$$\arg \max_{\beta_j} g(\alpha, \beta, \psi) = \lambda w_j - W \left(\lambda \exp(\lambda w_j) \sum_i \exp(\alpha_i) \exp(-\psi C_{ij} - 1) \right) \quad (10)$$

where W is the Lambert W function, which is defined as the inverse of $f(x) = xe^x$. Finally, since ψ cannot be solved for analytically, we can perform the following Newton step

$$\psi' = \psi - t \cdot \frac{\partial g / \partial \psi}{\partial^2 g / \partial \psi^2} \quad (11)$$

where

$$\begin{aligned} \partial g / \partial \psi &= -\epsilon + \sum_{ij} \exp(\alpha_i) C_{ij} \exp(-\psi C_{ij}) \exp(\beta_j) \\ \partial^2 g / \partial \psi^2 &= - \sum_{ij} \exp(\alpha_i) C_{ij}^2 \exp(-\psi C_{ij}) \exp(\beta_j) \end{aligned} \quad (12)$$

and where t is small enough such that $\psi' \geq 0$. Once we have solved the dual problem, we can recover the primal solution (to get the actual projection), which is described in Lemma 4 and proved in Appendix A.2.

Lemma 2. Suppose $\alpha^*, \beta^*, \psi^*$ maximize the dual problem g in Equation (16). Then,

$$\begin{aligned} z_i^* &= w_i - \beta_i / \lambda \\ \Pi_{ij}^* &= \exp(\alpha_i^*) \exp(-\psi^* C_{ij} - 1) \exp(\beta_j^*) \end{aligned} \quad (13)$$

are the corresponding solutions that minimize the primal problem in Equation (6).

The whole algorithm can then be vectorized and implemented as Algorithm 2, which we call projected Sinkhorn iterates. The algorithm uses a simple line search to ensure that the constraint $\psi \geq 0$ is not violated. Each iteration has $O(n^2)$ operations (matrix-vector product or matrix-matrix element-wise product), in comparison to the original Sinkhorn iteration which has 2 matrix-vector products.

Algorithm 2 Projected Sinkhorn iteration to project x onto the ϵ Wasserstein ball around y . We use \cdot to denote element-wise multiplication. The log and exp operators also apply element-wise.

```

input:  $x, w \in \mathbb{R}^n, C \in \mathbb{C}^{n \times n}, \lambda \in \mathbb{R}$ 
Initialize  $\alpha_i, \beta_i := \log(1/n)$  for  $i = 1, \dots, n$  and  $\psi := 1$ 
 $u, v := \exp(\alpha), \exp(\beta)$ 
while  $\alpha, \beta, \psi$  not converged do
    // update  $K$ 
     $K_\psi := \exp(-\psi C - 1)$ 

    // block coordinate descent iterates
     $\alpha := \log(x) - \log(K_\psi v)$ 
     $u := \exp(\alpha)$ 
     $\beta := \lambda w - W(u^T K_\psi \cdot \lambda \exp(\lambda w))$ 
     $v := \exp(\beta)$ 

    // Newton step
     $g := -\epsilon + u^T(C \cdot K_\psi)v$ 
     $h := -u^T(C \cdot C \cdot K_\psi)v$ 

    // ensure  $\psi \geq 0$ 
     $\alpha := 1$ 
    while  $\psi - \alpha g / h < 0$  do
         $\alpha := \alpha / 2$ 
    end while
     $\psi := \psi - \alpha g / h$ 
end while
return:  $w - \beta / \lambda$ 

```

Matrix scaling interpretation The original Sinkhorn iteration has a natural interpretation as a matrix scaling algorithm, iteratively rescaling the rows and columns of a matrix to achieve the target distributions. The Projected Sinkhorn iteration has a similar interpretation: while the α step rescales the rows of $\exp(-\psi C - 1)$ to sum to x , the β step rescales the columns of $\exp(-\psi C - 1)$ to sum to $-\beta/\lambda + w$, which is the primal transformation of the projected variable z at optimality as described in Lemma 4. Lastly, the ψ step can be interpreted as correcting for the transport cost of the current scaling: the numerator of the Newton step is simply the difference between the transport cost of the current matrix scaling and the maximum constraint ϵ . A full derivation of the algorithm and a more detailed explanation on this interpretation can be found in Appendix A.3.

4.2. Local Transport Plans

The quadratic runtime dependence on input dimension can grow quickly, and this is especially true for images. Rather than allowing transport plans to move mass to and from any pair of pixels, we instead restrict the transport plan to

Table 1. Classification accuracies for models used in the experiments.

DATA SET	MODEL	NOMINAL ACCURACY
MNIST	STANDARD	98.90%
	BINARIZE	98.73%
	ROBUST	98.20%
	ADV. TRAINING	96.95%
CIFAR10	STANDARD	94.70%
	ROBUST	66.33%
	ADV. TRAINING	80.69%

move mass only within a $k \times k$ region of the originating pixel, similar in spirit to a convolutional filter. As a result, the cost matrix C only needs to define the cost within a $k \times k$ region, and we can utilize tools used for convolutional filters to efficiently apply the cost to each $k \times k$ region. This reduces the computational complexity of each iteration to $O(nk^2)$. For images with more than one channel, we can use the same transport plan for each channel and only allow transport within a channel, so the cost matrix remains $k \times k$. For 5×5 local transport plans on CIFAR10, the projected Sinkhorn iterates typically converge in around 30-40 iterations, taking about 0.02 seconds per iteration on a Titan X for minibatches of size 100. Note that if we use a cost matrix C that reflects the 1-Wasserstein distance, then this problem could be solved even more efficiently using Kantrovich duality, however we use this formulation to enable more general p -Wasserstein distances, or even non-standard cost matrices.

Projected gradient descent on the Wasserstein ball

With local transport plans, the method is fast enough to be used within a projected gradient descent routine to generate adversarial examples on images, and further used for adversarial training as in Algorithm 1 (using steepest descent with respect to ℓ_∞ norm), except that we do an approximate projection onto the Wasserstein ball using Algorithm 2.

5. Results

In this section, we run the Wasserstein examples through a range of typical experiments in the literature of adversarial examples. Table 1 summarizes the nominal error rates obtained by all considered models. All experiments can be run on a single GPU, and all code for the experiments is available at https://github.com/locuslab/projected_sinkhorn.

Architectures For MNIST we used the convolutional ReLU architecture used in Wong & Kolter (2018), with two convolutional layers with 16 and 32 4×4 filters each, followed by a fully connected layer with 100 units, which achieves a nominal accuracy of 98.89%. For CIFAR10 we

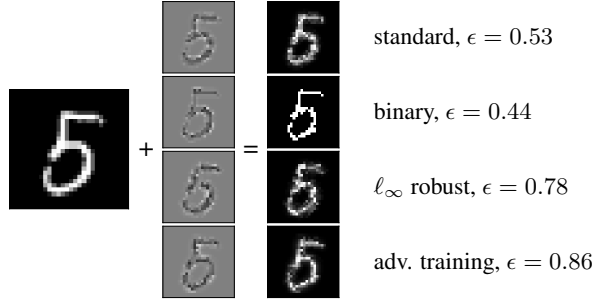


Figure 3. Wasserstein adversarial examples on the MNIST dataset for the four different models. Note that the ℓ_∞ robust and the adversarially trained models require a much larger ϵ radius for the Wasserstein ball in order to generate an adversarial example. Each model classifies the corresponding perturbed example as an 8 instead of a 5, except for the first one which classifies the perturbed example as a 6.

focused on the standard ResNet18 architecture (He et al., 2016), which achieves a nominal accuracy of 94.76%.

Hyperparameters For all experiments in this section, we focused on using 5×5 local transport plans for the Wasserstein ball, and used an entropy regularization constant of 1000 for MNIST and 3000 for CIFAR10. The cost matrix used for transporting between pixels is taken to be the 2-norm of the distance in pixel space (e.g. the cost of going from pixel (i, j) to (k, l) is $\sqrt{|i - j|^2 + |k - l|^2}$), which makes the optimal transport cost a metric more formally known as the 1-Wasserstein distance. For more extensive experiments on using different sizes of transport plans, different regularization constants, and different cost matrices, we direct the reader to Appendix C.

Evaluation at test time We use the follow evaluation procedure to attack models with projected gradient descent on the Wasserstein ball. For each MNIST example, we start with $\epsilon = 0.3$ and increase it by a factor of 1.1 every 10 iterations until either an adversarial example is found or until 200 iterations have passed, allowing for a maximum perturbation radius of $\epsilon = 2$. For CIFAR10, we start with $\epsilon = 0.001$ and increase it by a factor of 1.17 until either an adversarial example is found or until 400 iterations have passed, allowing for a maximum perturbation radius of $\epsilon = 0.53$.

5.1. MNIST

For MNIST, we consider a standard model, a model with binarization, a model provably robust to ℓ_∞ perturbations of at most $\epsilon = 0.1$, and an adversarially trained model. We provide a visual comparison of the Wasserstein adversarial examples generated on each of the four models in Figure 3. The susceptibility of all four models to the Wasserstein attack is plotted in Figure 4.

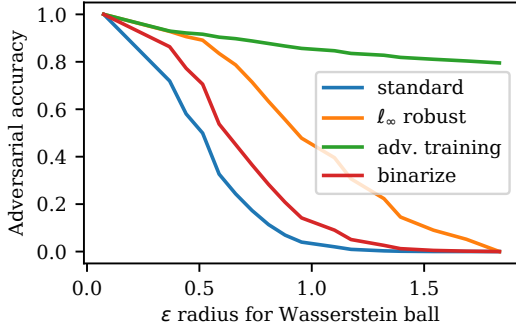


Figure 4. Adversarial accuracy of various models on MNIST when attacked by a Wasserstein adversary over varying sizes of ϵ -Wasserstein balls. We find that all models not trained with adversarial training against this attack eventually achieve 0% accuracy, however we do observe that models trained to be provably robust against ℓ_∞ perturbations are still somewhat more robust than standard models, or models utilizing binarization as a defense.

Standard model and binarization For MNIST, despite restricting the transport plan to local 5×5 regions, a standard model is easily attacked by Wasserstein adversarial examples. In Figure 4, we see that Wasserstein attacks with $\epsilon = 0.5$ can successfully attack a typical MNIST classifier 50% of the time, which goes up to 94% for $\epsilon = 1$. A Wasserstein radius of $\epsilon = 0.5$ can be intuitively understood as moving 50% of the pixel mass over by 1 pixel, or alternatively moving less than 50% of the pixel mass more than 1 pixel. Furthermore, while preprocessing images with binarization is often seen as a way to trivialize adversarial examples on MNIST, we find that it performs only marginally better than the standard model against Wasserstein perturbations.

ℓ_∞ robust model We also run the attack on the model trained by Wong et al. (2018), which is guaranteed to be provably robust against ℓ_∞ perturbations with $\epsilon \leq 0.1$. While not specifically trained against Wasserstein perturbations, in Figure 4 we find that it is substantially more robust than either the standard or the binarized model, requiring a significantly larger ϵ to have the same attack success rate.

Adversarial training Finally, we apply this attack as an inner procedure within an adversarial training framework for MNIST. To save on computation, during training we adopt a weaker adversary and use only 50 iterations of projected gradient descent. We also let ϵ grow within a range and train on the first adversarial example found (essentially a budget version of the attack used at test time). Specific details regarding this ϵ schedule and also the learning parameters used can be found in Appendix B.1. We find that the adversarially trained model is empirically the most well defended against this attack of all four models, and cannot be attacked down to 0% accuracy (Figure 4).

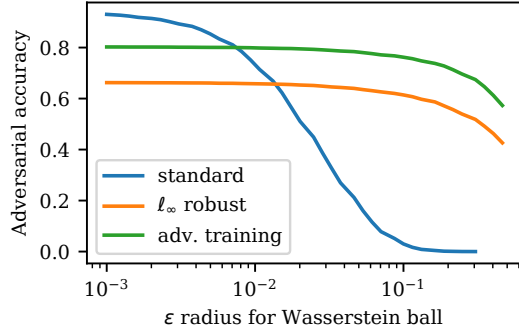


Figure 5. Adversarial accuracy of various models on the CIFAR10 dataset when attacked by a Wasserstein adversary. We find that the model trained to be robust against ℓ_∞ perturbations is actually more robust than adversarial training.

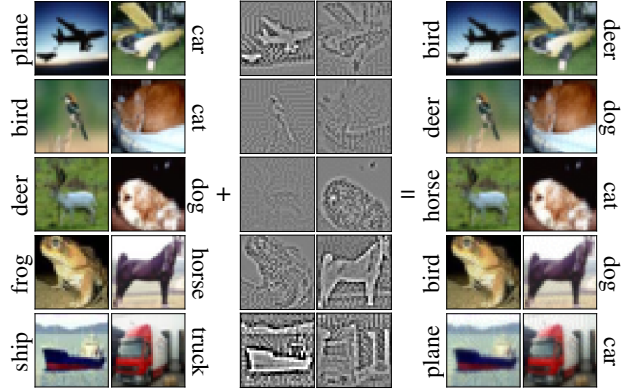


Figure 6. Wasserstein adversarial examples for CIFAR10 on a typical ResNet18 for all 10 classes. The perturbations here represents the total change across all three channels, where total change is plotted within the range ± 0.165 (the maximum total change observed in a single pixel) for images scaled to [0,1].

5.2. CIFAR10

For CIFAR10, we consider a standard model, a model provably robust to ℓ_∞ perturbations of at most $\epsilon = 2/255$, and an adversarially trained model. We plot the susceptibility of each model to the Wasserstein attack in Figure 5.

Standard model We find that for a standard ResNet18 CIFAR10 classifier, a perturbation radius of as little as 0.01 is enough to misclassify 25% of the examples, while a radius of 0.1 is enough to fool the classifier 97% of the time (Figure 5). Despite being such a small ϵ , we see in Figure 6 that the structure of the perturbations still reflect the actual content of the images, though certain classes require larger magnitudes of change than others.

ℓ_∞ robust model We further empirically evaluate the attack on a model that was trained to be provably robust against ℓ_∞ perturbations. We use the models weights from Wong et al. (2018), which are trained to be provably robust

against ℓ_∞ perturbations of at most $\epsilon = 2/255$. Further note that this CIFAR10 model actually is a smaller ResNet than the ResNet18 architecture considered in this paper, and consists of 4 residual blocks with 16, 16, 32, and 64 filters. Nonetheless, we find that while the model suffers from poor nominal accuracy (achieving only 66% accuracy on unperturbed examples as noted in Table 1), the robustness against ℓ_∞ attacks remarkably seems to transfer quite well to robustness against Wasserstein attacks in the CIFAR10 setting, achieving 61% adversarial accuracy for $\epsilon = 0.1$ in comparison to 3% for the standard model.

Adversarial training To perform adversarial training for CIFAR10, we use a similar scheme to that used for MNIST: we adopt a weaker adversary that uses only 50 iterations of projected gradient descent during training and allow ϵ to grow within a range (specific details can be found in Appendix B.2). We find that adversarial training here is also able to defend against this attack, and at the same threshold of $\epsilon = 0.1$, we find that the adversarial accuracy has been improved from 3% to 76%.

5.3. Provable Defenses against Wasserstein Perturbations

Lastly, we present some analysis on how this attack fits into the context of provable defenses, along with a negative result demonstrating a fundamental gap that needs to be solved. The Wasserstein attack can be naturally incorporated into duality based defenses: Wong et al. (2018) show that to use their certificates to defend against other inputs, one only needs to solve the following optimization problem:

$$\max_{x \in B(x, \epsilon)} -x^T y \quad (14)$$

for some constant y and for some perturbation region $B(x, \epsilon)$ (a similar approach can be taken to adapt the dual verification from Dvijotham et al. (2018)). For the Wasserstein ball, this is highly similar to the problem of projecting onto the Wasserstein ball from Equation (6), with a linear objective instead of a quadratic objective and fewer variables. In fact, a Sinkhorn-like algorithm can be derived to solve this problem, which ends up being a simplified version of Algorithm 2 (this is shown in Appendix D).

However, there is a fundamental obstacle towards generating provable certificates against Wasserstein attacks: these defenses (and many other, non-duality based approaches) depend heavily on propagating interval bounds from the input space through the network, in order to efficiently bound the output of ReLU units. This concept is inherently at odds with the notion of Wasserstein distance: a “small” Wasserstein ball can use a low-cost transport plan to move all the mass at a single pixel to its neighbors, or vice versa. As a result, when converting a Wasserstein ball to interval con-

straints, the interval bounds immediately become vacuous: each individual pixel can attain their minimum or maximum value under some ϵ cost transport plan. In order to guarantee robustness against Wasserstein adversarial attacks, significant progress must be made to overcome this limitation.

6. Conclusion

In this paper, we have presented a new, general threat model for adversarial examples based on the Wasserstein distance, a metric that captures a kind of perturbation that is fundamentally different from traditional ℓ_p perturbations. To generate these examples, we derived an algorithm for fast, approximate projection onto the Wasserstein ball that can use local transport plans for even more speedup on images. We successfully attacked standard networks, showing that these adversarial examples are structurally perturbed according to the content of the image, and demonstrated the empirical effectiveness of adversarial training. Finally, we observed that networks trained to be provably robust against ℓ_∞ attacks are more robust than the standard networks against Wasserstein attacks, however we show that the current state of provable defenses is insufficient to directly apply to the Wasserstein ball due to their reliance on interval bounds.

We believe overcoming this roadblock is crucial to the development of verifiers or provable defenses against not just the Wasserstein attack, but also to improve the robustness of classifiers against other attacks that do not naturally convert to interval bounds (e.g. ℓ_0 or ℓ_1 attacks). Whether we can develop efficient verification or provable training methods that do not rely on interval bounds remains an open question.

Perhaps the most natural future direction for this work is to begin to understand the properties of Wasserstein adversarial examples and what we can do to mitigate them, even if only at a heuristic level. However, at the end of the day, the Wasserstein threat model defines just one example of a convex region capturing structure that is different from ℓ_p balls. By no means have we characterized all reasonable adversarial perturbations, and so a significant gap remains in determining how to rigorously define general classes of adversarial examples that can characterize phenomena different from the ℓ_p and Wasserstein balls.

Finally, although we focused primarily on adversarial examples in this work, the method of projecting onto Wasserstein balls may be applicable outside of deep learning. Projection operators play a major role in optimization algorithms beyond projected gradient descent (e.g. ADMM and alternating projections). Perhaps even more generally, the techniques in this paper could be used to derive Sinkhorn-like algorithms for classes of problems that consider Wasserstein constrained variables.

References

- Altschuler, J., Weed, J., and Rigollet, P. Near-linear time approximation algorithms for optimal transport via sinkhorn iteration. In *Advances in Neural Information Processing Systems*, pp. 1964–1974, 2017.
- Athalye, A., Carlini, N., and Wagner, D. Obfuscated gradients give a false sense of security: Circumventing defenses to adversarial examples. In *Proceedings of the 35th International Conference on Machine Learning, ICML 2018*, July 2018a. URL <https://arxiv.org/abs/1802.00420>.
- Athalye, A., Engstrom, L., Ilyas, A., and Kwok, K. Synthesizing robust adversarial examples. In Dy, J. and Krause, A. (eds.), *Proceedings of the 35th International Conference on Machine Learning*, volume 80 of *Proceedings of Machine Learning Research*, pp. 284–293, Stockholm, Sweden, 10–15 Jul 2018b. PMLR. URL <http://proceedings.mlr.press/v80/athalye18b.html>.
- Carlini, N. and Wagner, D. Towards evaluating the robustness of neural networks. In *Security and Privacy (SP), 2017 IEEE Symposium on*, pp. 39–57. IEEE, 2017.
- Croce, F., Andriushchenko, M., and Hein, M. Provable robustness of relu networks via maximization of linear regions. *CoRR*, abs/1810.07481, 2018. URL <https://arxiv.org/abs/1810.07481>.
- Cuturi, M. Sinkhorn distances: Lightspeed computation of optimal transport. In Burges, C. J. C., Bottou, L., Welling, M., Ghahramani, Z., and Weinberger, K. Q. (eds.), *Advances in Neural Information Processing Systems 26*, pp. 2292–2300. Curran Associates, Inc., 2013. URL <http://papers.nips.cc/paper/4927-sinkhorn-distances-lightspeed-computation-of-optimal-transport.pdf>.
- Dvijotham, K., Stanforth, R., Gowal, S., Mann, T., and Kohli, P. A dual approach to scalable verification of deep networks. In *Proceedings of the Thirty-Fourth Conference Annual Conference on Uncertainty in Artificial Intelligence (UAI-18)*, pp. 162–171, Corvallis, Oregon, 2018. AUAI Press.
- Engstrom, L., Tran, B., Tsipras, D., Schmidt, L., and Madry, A. A rotation and a translation suffice: Fooling cnns with simple transformations. *arXiv preprint arXiv:1712.02779*, 2017.
- Eykholt, K., Evtimov, I., Fernandes, E., Li, B., Rahmati, A., Xiao, C., Prakash, A., Kohno, T., and Song, D. Robust physical-world attacks on deep learning visual classification. In *Proceedings of the IEEE Conference on Computer Vision and Pattern Recognition*, pp. 1625–1634, 2018.
- Goodfellow, I., Shlens, J., and Szegedy, C. Explaining and harnessing adversarial examples. In *International Conference on Learning Representations*, 2015. URL <http://arxiv.org/abs/1412.6572>.
- Gowal, S., Dvijotham, K., Stanforth, R., Bunel, R., Qin, C., Uesato, J., Arandjelovic, R., Mann, T. A., and Kohli, P. On the effectiveness of interval bound propagation for training verifiably robust models. *CoRR*, abs/1810.12715, 2018. URL <http://arxiv.org/abs/1810.12715>.
- He, K., Zhang, X., Ren, S., and Sun, J. Deep residual learning for image recognition. In *Proceedings of the IEEE conference on computer vision and pattern recognition*, pp. 770–778, 2016.
- Kurakin, A., Goodfellow, I., and Bengio, S. Adversarial examples in the physical world. *ICLR Workshop*, 2017. URL <https://arxiv.org/abs/1607.02533>.
- Lu, J., Sibai, H., Fabry, E., and Forsyth, D. No need to worry about adversarial examples in object detection in autonomous vehicles. *arXiv preprint arXiv:1707.03501*, 2017.
- Madry, A., Makelov, A., Schmidt, L., Tsipras, D., and Vladu, A. Towards deep learning models resistant to adversarial attacks. In *International Conference on Learning Representations*, 2018. URL <https://openreview.net/forum?id=rJzIBfZAb>.
- Mirman, M., Gehr, T., and Vechev, M. Differentiable abstract interpretation for provably robust neural networks. In *International Conference on Machine Learning (ICML)*, 2018. URL <https://www.icml.cc/Conferences/2018/Schedule?showEvent=2477>.
- Papernot, N., McDaniel, P., Wu, X., Jha, S., and Swami, A. Distillation as a defense to adversarial perturbations against deep neural networks. In *Security and Privacy (SP), 2016 IEEE Symposium on*, pp. 582–597. IEEE, 2016.
- Raghunathan, A., Steinhardt, J., and Liang, P. S. Semidefinite relaxations for certifying robustness to adversarial examples. In Bengio, S., Wallach, H., Larochelle, H., Grauman, K., Cesa-Bianchi, N., and Garnett, R. (eds.), *Advances in Neural Information Processing Systems 31*, pp. 10900–10910. Curran Associates, Inc., 2018. URL <http://papers.nips.cc/paper/8285-semidefinite-relaxations-for-certifying-robustness-to-adversarial-examples.pdf>.

Sharif, M., Bhagavatula, S., Bauer, L., and Reiter, M. K. Adversarial generative nets: Neural network attacks on state-of-the-art face recognition. *arXiv preprint arXiv:1801.00349*, 2017.

Sinha, A., Namkoong, H., and Duchi, J. Certifying some distributional robustness with principled adversarial training. 2018.

Szegedy, C., Zaremba, W., Sutskever, I., Bruna, J., Erhan, D., Goodfellow, I., and Fergus, R. Intriguing properties of neural networks. In *International Conference on Learning Representations*, 2014. URL <http://arxiv.org/abs/1312.6199>.

Tjeng, V., Xiao, K. Y., and Tedrake, R. Evaluating robustness of neural networks with mixed integer programming. In *International Conference on Learning Representations*, 2019. URL <https://openreview.net/forum?id=HyGIdiRqtm>.

Wong, E. and Kolter, Z. Provable defenses against adversarial examples via the convex outer adversarial polytope. In *International Conference on Machine Learning*, pp. 5283–5292, 2018.

Wong, E., Schmidt, F., Metzen, J. H., and Kolter, J. Z. Scaling provable adversarial defenses. In Bengio, S., Wallach, H., Larochelle, H., Grauman, K., Cesa-Bianchi, N., and Garnett, R. (eds.), *Advances in Neural Information Processing Systems 31*, pp. 8410–8419. Curran Associates, Inc., 2018. URL <http://papers.nips.cc/paper/8060-scaling-provable-adversarial-defenses.pdf>.

Xiao, K. Y., Tjeng, V., ShafiuIlah, N. M. M., and Madry, A. Training for faster adversarial robustness verification via inducing ReLU stability. In *International Conference on Learning Representations*, 2019. URL <https://openreview.net/forum?id=BJfIVjAcKm>.

A. Projected Sinkhorn derivation

A.1. Proof of Lemma 3

Lemma 3. *The dual of the entropy-regularized Wasserstein projection problem in Equation (6) is*

$$\underset{\alpha, \beta \in \mathbb{R}^n, \psi \in \mathbb{R}_+}{\text{maximize}} \quad g(\alpha, \beta, \psi) \quad (15)$$

where

$$\begin{aligned} g(\alpha, \beta, \psi) = & -\frac{1}{2\lambda} \|\beta\|_2^2 - \psi\epsilon + \alpha^T x + \beta^T w \\ & - \sum_{ij} \exp(\alpha_i) \exp(-\psi C_{ij} - 1) \exp(\beta_j) \end{aligned} \quad (16)$$

Proof. For convenience, we multiply the objective by λ and solve this problem instead:

$$\begin{aligned} & \underset{z \in \mathbb{R}_+^n, \Pi \in \mathbb{R}_+^{n \times n}}{\text{minimize}} \quad \frac{\lambda}{2} \|w - z\|_2^2 + \sum_{ij} \Pi_{ij} \log(\Pi_{ij}) \\ & \text{subject to} \quad \Pi 1 = x \\ & \quad \Pi^T 1 = z \\ & \quad \langle \Pi, C \rangle \leq \epsilon. \end{aligned} \quad (17)$$

Introducing dual variables (α, β, ψ) where $\psi \geq 0$, the Lagrangian is

$$\begin{aligned} L(z, \Pi, \alpha, \beta, \psi) = & \frac{\lambda}{2} \|w - z\|_2^2 + \sum_{ij} \Pi_{ij} \log(\Pi_{ij}) + \psi(\langle \Pi, C \rangle - \epsilon) \\ & + \alpha^T(x - \Pi 1) + \beta^T(z - \Pi^T 1). \end{aligned} \quad (18)$$

The KKT optimality conditions are now

$$\begin{aligned} \frac{\partial L}{\partial \Pi_{ij}} &= \psi C_{ij} + (1 + \log(\Pi_{ij})) - \alpha_i - \beta_j = 0 \\ \frac{\partial L}{\partial z_j} &= \lambda(z_j - w_j) + \beta_j = 0 \end{aligned} \quad (19)$$

so at optimality, we must have

$$\begin{aligned} \Pi_{ij} &= \exp(\alpha_i) \exp(-\psi C_{ij} - 1) \exp(\beta_j) \\ z &= -\frac{\beta}{\lambda} + w \end{aligned} \quad (20)$$

Plugging in the optimality conditions, we get

$$\begin{aligned} L(z^*, \Pi^*, \alpha, \beta, \psi) &= -\frac{1}{2\lambda} \|\beta\|_2^2 - \psi\epsilon + \alpha^T x + \beta^T w \\ & - \sum_{ij} \exp(\alpha_i) \exp(-\psi C_{ij} - 1) \exp(\beta_j) \\ & = g(\alpha, \beta, \psi) \end{aligned} \quad (21)$$

so the dual problem is to maximize g over $\alpha, \beta, \psi \geq 0$. \square

A.2. Proof of Lemma 4

Lemma 4. *Suppose $\alpha^*, \beta^*, \psi^*$ maximize the dual problem g in Equation (16). Then,*

$$\begin{aligned} z_i^* &= w_i - \beta_i / \lambda \\ \Pi_{ij}^* &= \exp(\alpha_i^*) \exp(-\psi^* C_{ij} - 1) \exp(\beta_j^*) \end{aligned} \quad (22)$$

are the corresponding solutions that minimize the primal problem in Equation (6).

Proof. These equations follow directly from the KKT optimality conditions from Equation (20). \square

A.3. Algorithm derivation and interpretation

Derivation To derive the algorithm, note that since this is a strictly convex problem to get the α and β iterates we solve for setting the gradient to 0. The derivative with respect to α is

$$\frac{\partial g}{\partial \alpha_i} = x_i - \exp(\alpha_i) \sum_j \exp(-\psi C_{ij} - 1) \exp(\beta_j) \quad (23)$$

and so setting this to 0 and solving for α_i gives the α iterate. The derivative with respect to β is

$$\frac{\partial g}{\partial \beta_j} = -\frac{1}{\lambda} \beta_j + w_j - \exp(\beta_j) \sum_i \exp(\alpha_i) \exp(-\psi C_{ij} - 1) \quad (24)$$

and setting this to 0 and solving for β_j gives the β iterate (this step can be done using a symbolic solver, we used Mathematica). Lastly, the ψ updates are straightforward scalar calculations of the derivative and second derivative.

Interpretation Recall from the transformation of dual to primal variables from Lemma 4. To see how the Projected Sinkhorn iteration is a (modified) matrix scaling algorithm, we can interpret these quantities before optimality as primal iterates. Namely, at each iteration t , let

$$\begin{aligned} z_i^{(t)} &= w_i - \beta_i^{(t)} / \lambda \\ \Pi_{ij}^{(t)} &= \exp(\alpha^{(t)}) \exp(-\psi^{(t)} C_{ij} - 1) \exp(\beta^{(t)}) \end{aligned} \quad (25)$$

Then, since the α and β steps are equivalent to setting Equations (23) and (24) to 0, we know that after an update for $\alpha^{(t)}$, we have that

$$x_i = \sum_j \Pi_{ij}^{(t)} \quad (26)$$

so the α step rescales the transport matrix to sum to x . Similarly, after an update for $\beta^{(t)}$, we have that

$$z_i^{(t)} = \sum_i \Pi_{ij}^{(t)} \quad (27)$$

which is a rescaling of the transport matrix to sum to the projected value. Lastly, the numerator of the $\psi^{(t)}$ step can be rewritten as

$$\psi^{(t+1)} = \psi^{(t)} + t \cdot \frac{\langle \Pi^{(t)}, C \rangle - \epsilon}{\langle \Pi^{(t)}, C \cdot C \rangle} \quad (28)$$

as a simple adjustment based on whether the current transport plan $\Pi^{(t)}$ is above or below the maximum threshold ϵ .

B. Experimental setup

B.1. MNIST

Adaptive ϵ During adversarial training for MNIST, we adopt an adaptive ϵ scheme to avoid selecting a specific ϵ . Specifically, to find an adversarial example, we first let $\epsilon = 0.1$ on the first iteration of projected gradient descent, and increase it by a factor of 1.4 every 5 iterations. We terminate the projected gradient descent algorithm when either an adversarial example is found, or when 50 iterations have passed, allowing ϵ to take on values in the range $[0.1, 2.1]$

Optimizer hyperparameters To update the model weights during adversarial training, we use the SGD optimizer with 0.9 momentum and 0.0005 weight decay, and batch sizes of 128. We begin with a learning rate of 0.1, reduce it to 0.01 after 10 epochs.

B.2. CIFAR10

Adaptive ϵ We also use an adaptive ϵ scheme for adversarial training in CIFAR10. Specifically, we let $\epsilon = 0.01$ on the first iteration of projected gradient descent, and increase it by a factor of 1.5 every 5 iterations. Similar to MNIST, we terminate the projected gradient descent algorithm when either an adversarial example is found, or 50 iterations have passed, allowing ϵ to take on values in the range $[0.01, 0.38]$.

Optimizer hyperparameters Similar to MNIST, to update the model weights, we use the SGD optimizer with 0.9 momentum and 0.0005 weight decay, and batch sizes of 128. The learning rate is also the same as in MNIST, starting at 0.1, and reducing to 0.01 after 10 epochs.

B.3. Motivation for adaptive ϵ

A commonly asked question of models trained to be robust against adversarial examples is “what if the adversary has a perturbation budget of $\epsilon + \delta$ instead of ϵ ?” This is referring to a “robustness cliff,” where a model trained against an ϵ strong adversary has a sharp drop in robustness when attacked by an adversary with a slightly larger budget. To address this, we advocate for the slightly modified version of typical adversarial training used in this work: rather than

picking a fixed ϵ and running projected gradient descent, we instead allow for an adversarial to have a range of $\epsilon \in [\epsilon_{min}, \epsilon_{max}]$. To do this, we begin with $\epsilon = \epsilon_{min}$, and then gradually increase it by a multiplicative factor γ until either an adversarial example is found or until ϵ_{max} is reached. While similar ideas have been used before for evaluating model robustness, we specifically advocate for using this schema *during adversarial training*. This has the advantage of extending robustness of the classifier beyond a single ϵ threshold, allowing a model to achieve a potentially higher robustness threshold while not being significantly harmed by “impossible” adversarial examples.

C. Auxiliary experiments

In this section, we explore the space of possible parameters that we treated as fixed in the main paper. While this is not an exhaustive search, we hope to provide some intuition as to why we chose the parameters we did.

C.1. Effect of λ and C

We first study the effect of λ and the cost matrix C . First, note that λ could be any positive value. Furthermore, note that to construct C we used the 2-norm which reflects the 1-Wasserstein metric, but in theory we could use any p -Wasserstein metric, where the cost of moving from pixel (i, j) to (k, l) is $(|i - j|^2 + |k - l|^2)^{p/2}$. Figure 8 shows the effects of λ and p on both the adversarial example and the radius at which it was found for varying values of $\lambda = [1, 10, 100, 500, 1000]$ and $p = [1, 2, 3, 4, 5]$.

We find that it is important to ensure that λ is large enough, otherwise the projection of the image is excessively blurred. In addition to qualitative changes, smaller λ seems to make it harder to find Wasserstein adversarial examples, making the ϵ radius go up as λ gets smaller. In fact, for $\lambda = (1, 10)$ and almost all of $\lambda = 100$, the blurring is so severe that no adversarial example can be found.

In contrast, we find that increasing p for the Wasserstein distance used in the cost matrix C seems to make the images more “blocky”. Specifically, as p gets higher tested, more pixels seem to be moved in larger amounts. This seems to counteract the blurring observed for low λ to some degree. Naturally, the ϵ radius also grows since the overall cost of the transport plan has gone up.

C.2. Size of local transport plan

In this section we explore the effects of different sized transport plans. In the main paper, we used a 5×5 local transport plan, but this could easily be something else, e.g. 3×3 or 7×7 . We can see a comparison on the robustness of a standard and the ℓ_∞ robust model against these different sized

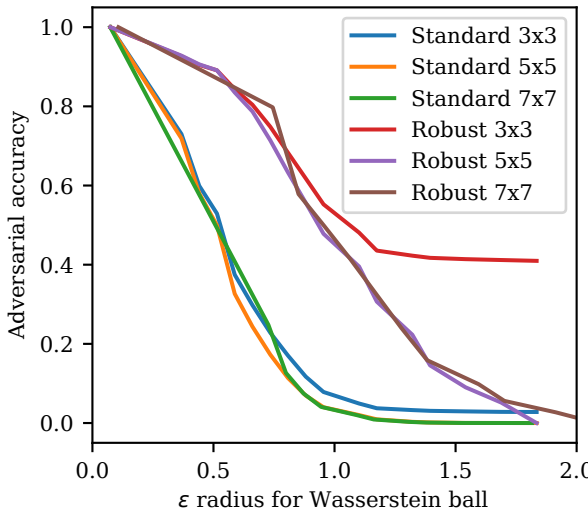


Figure 7. Adversarial accuracy of a standard model and a model trained to be provably robust against ℓ_∞ attacks for different sizes of transport plans. In most cases the size of the transport plan doesn't seem to matter, except for the 3×3 local transport plan. In this case, the adversary isn't quite able to reach 0% accuracy for the standard model, reaching 2.8% for $\epsilon = 1.83$. The adversary is also unable to attack the robust MNIST model, bottoming out at 41% adversarial accuracy at $\epsilon = 1.83$.

transport plans in Figure 7, using $\lambda = 1000$. We observe that while 3×3 transport plans have difficulty attacking the robust MNIST model, all other plan sizes seem to have similar performance.

D. Provable defense

In this section we show how a Sinkhorn-like algorithm can be derived for provable defenses, and that the resulting algorithm is actually just a simplified version of the Projected Sinkhorn iteration, which we call the Conjugate Sinkhorn iteration (since it solves the conjugate problem).

D.1. Conjugate Sinkhorn iteration

By subtracting the same entropy term to the conjugate objective from Equation (14), we can get a problem similar to that of projecting onto the Wasserstein ball.

$$\begin{aligned} & \underset{z \in \mathbb{R}_+^n, \Pi \in \mathbb{R}_+^{n \times n}}{\text{minimize}} && -\lambda z^T y + \sum_{ij} \Pi_{ij} \log(\Pi_{ij}) \\ & \text{subject to} && \Pi 1 = x \\ & && \Pi^T 1 = z \\ & && \langle \Pi, C \rangle \leq \epsilon. \end{aligned} \tag{29}$$

where again we've multiplied the objective by λ for convenience. Following the same framework as before, we introduce dual variables (α, β, ψ) where $\psi \geq 0$, to con-

struct the Lagrangian as

$$\begin{aligned} & L(z, \Pi, \alpha, \beta, \psi) \\ &= -\lambda z^T y + \sum_{ij} \Pi_{ij} \log(\Pi_{ij}) + \psi(\langle \Pi, C \rangle - \epsilon) \\ & \quad + \alpha^T (x - \Pi 1) + \beta^T (z - \Pi^T 1). \end{aligned} \tag{30}$$

Note that since all the terms with Π_{ij} are the same, the corresponding KKT optimality condition for Π_{ij} also remains the same. The only part that changes is the optimality condition for z , which becomes

$$\beta = \lambda y \tag{31}$$

Plugging the optimality conditions into the Lagrangian, we get the following dual problem:

$$\begin{aligned} & L(z^*, \Pi^*, \alpha, \beta, \psi) \\ &= -\psi \epsilon + \alpha^T x \\ & \quad - \sum_{ij} \exp(\alpha_i) \exp(-\psi C_{ij} - 1) \exp(\beta_j) \\ &= g(\alpha, \psi) \end{aligned} \tag{32}$$

Finally, if we minimize this with respect to α and ψ we get exactly the same update steps as the Projected Sinkhorn iteration. Consequently, the Conjugate Sinkhorn iteration is identical to the Projected Sinkhorn iteration except that we replace the β step with the fixed value $\beta = \lambda y$.

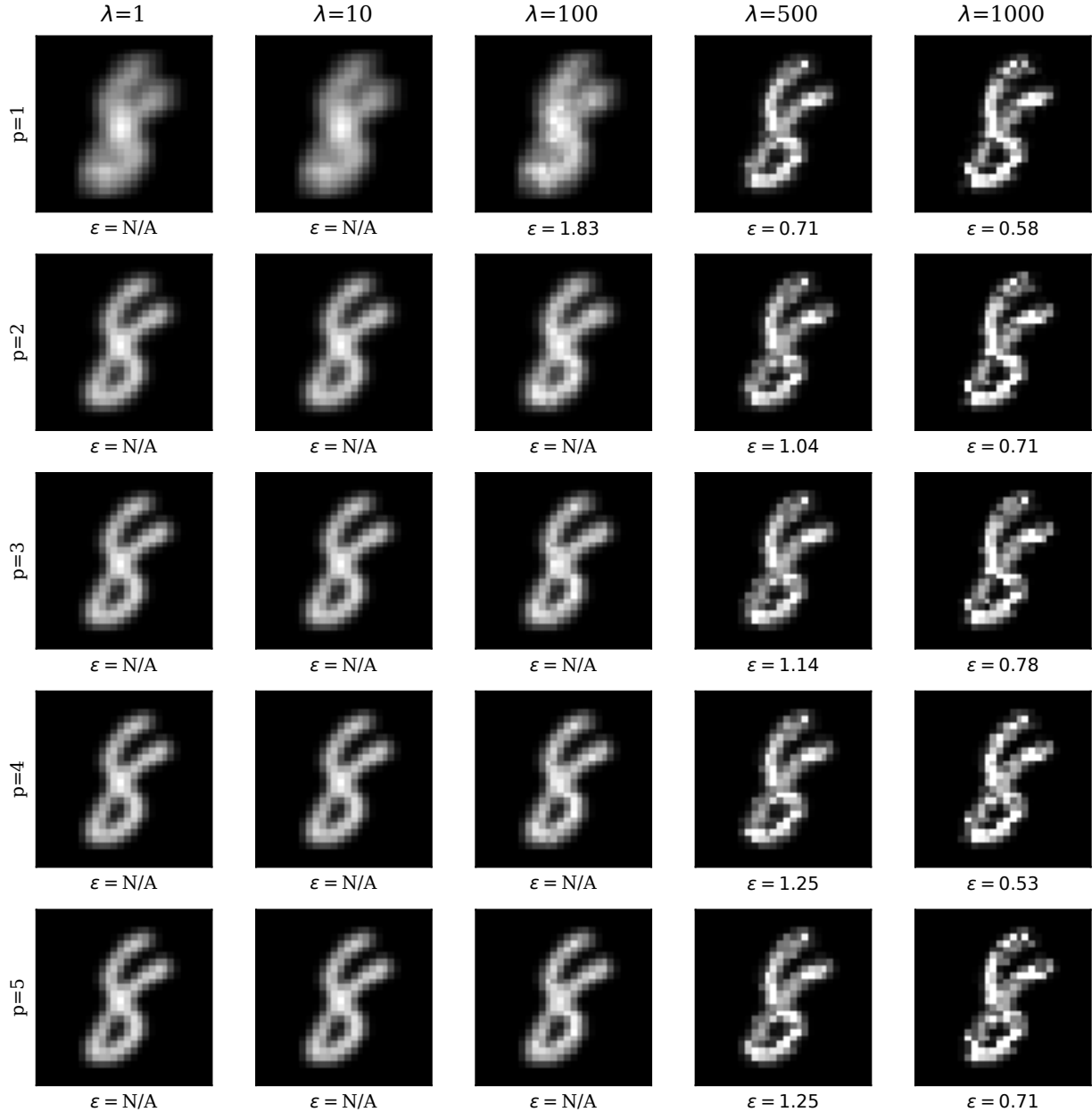


Figure 8. A plot of the adversarial examples generated with different p -Wasserstein metrics used for the cost matrix C and different regularization parameters λ . Note that when regularization is low, the image becomes blurred, and it is harder to find adversarial examples. In contrast, changing p does not seem to make any significant changes.